ORBIT – Open X-ray Scanner for Image-guided Interventional Surgery – Development of Concept

Fabian Stopp[1], Marc Käseberg[2], Christian Winne[2], Björn Marx[3], Jürgen Dehler[4] and Erwin Keeve[1, 2, *]

[1] Klinik für Mund-, Kiefer- und Gesichtschirurgie / Klinische Navigation
Charité – Universitätsmedizin Berlin
Augustenburger Platz 1
13353 Berlin

[2] Fraunhofer-Institut für Produktionsanlagen und Konstruktionstechnik IPK
Pascalstr. 8-9
10587 Berlin

[3]Center for Musculoskeletal Surgery
Charité – Universitätsmedizin Berlin
Augustenburger Platz 1
13353 Berlin

[4]Ziehm Imaging GmbH
Donaustr. 31
90451 Nürnberg

*Corresponding author email: keeve@charite.de

Abstract: Conventional 3D x-ray imaging systems, like CTs and 3D C-arms, are characterized by a circular movement of x-ray source and image detector around the patient. Using this technique the radiographed volume is reconstructed accurately, but the patient is fully enclosed and the access for the surgeon is limited. To improve the usability of intraoperative 3D imaging, we developed a new image acquisition method by optimizing the directions of x-ray projections within a limited angle range above the patient. The optimization method is based on the determinability of density changes inside a volume depending on the used directions of x-ray projections. The resulting orbital x-ray source trajectory allows an open system concept of a 3D x-ray scanner that ensures free access to the patient. Using a simulation environment and an experimental set-up we analyzed the developed image acquisition method and compared it with conventional trajectories. The results demonstrate the feasibility and usability of the proposed imaging method.

erschienen im Tagungsband der INFORMATIK 2011
Lecture Notes in Informatics, Band P192
ISBN 978-3-88579-286-4

1 Introduction

During surgical interventions three-dimensional (3D) x-ray imaging provides intraoperative control of implant placement and bone fracture repositioning. An important and useful application is the treatment of fractures, tumors or instabilities in spine surgery. To stabilize spine fractures adjacent vertebral bodies will be fixed permanently by the insertion of pedicle screws [Sc04][Be09]. During this process the spinal canal with spinal cord and sensitive nerve fibres inside of the vertebral bodies must not be injured by the screws (Figure 1). Because of the missing depth information two-dimensional x-ray projection images are not sufficient to detect misplaced screws [Be97]. Only 3D image information allows an accurate verification of the correct implant placement [LSG10]. To identify and revise misplaced implants during the intervention and to avoid cost-intensive re-interventions, 3D x-ray imaging has to be applied intraoperatively [Ke09]. But in spite of a great clinical need for intraoperative 3D x-ray imaging, special surgical requirements are not yet fulfilled. The spatial limitations in a crowded operating room and the surgical demand for free access to the patient have to be more considered by the intraoperative 3D x-ray imaging techniques.

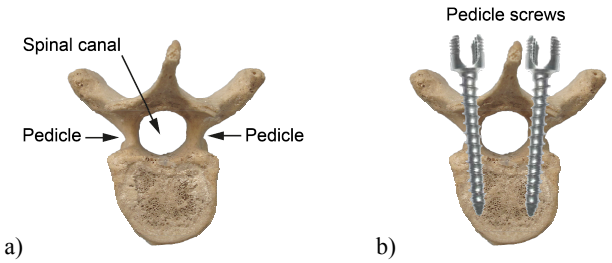

Figure 1: a) Pedicles and spinal canal of a thoracic vertebral body; b) Insertion of pedicle screws in a thoracic vertebral body

In computed tomography a volume is 3D reconstructed using x-ray projection images of the volume acquired from different directions. Conventional 3D x-ray imaging systems are characterized by a rigid configuration of x-ray source and image detector and a circular rotation around the patient. Using this technique, the radiographed volume is reconstructed accurately, but the patient is fully enclosed and the access for the surgeon is restricted. This leads to an interruption of the surgical workflow because the imaging systems normally cannot remain at the patient during the intervention. It takes several minutes to move the system to the operating table and align it to the patient. For a reapplication of 3D imaging this process has to be repeated and the surgery has to be interrupted again.

1.1 Commercial intraoperative 3D x-ray systems

Today two main groups of commercial 3D x-ray systems for surgery exist: computer tomographs (CTs) and 3D C-arms.

CT systems consist of a closed circular gantry in which x-ray source and image detector are rotating around the patient. CTs provide a high image quality but their design and physical dimension are disadvantageous for intraoperative use. The “Dominion” (Imaging3 Inc), a small tiltable mobile CT, and the “O-arm” (Medtronic) are some specialized CTs for intraoperative application. In contrast to conventional CT systems the gantry of the O-arm can be opened to align the system at the patient table. For 3D imaging the gantry is closed and x-ray source and image detector are rotating 360° inside of the gantry.

3D C-arms are characterized by a C-sharped structure with mounted x-ray source and image detector (Figure 2a). For 3D imaging the axes of the C-arm are motorized and the C-structure is rotating around the patient. New generations of 3D C-arms use digital flat panel detectors to provide an enlarged and distortion free volume reconstruction (Figure 2b). A new development is the robot-guided C-arm “Artis zeego” (Siemens) for angiography and computed tomography. The floor mounted robot arm allows a flexible C-arm positioning at the patient table, but the C-sharped structure is still rotating around the patient for 3D imaging.

a)  b) 

Figure 2: Intraoperative use of 3D C-arms at the Charité – Universitätsmedizin Berlin

1.2 Alternative image acquisition methods

To improve intraoperative 3D x-ray imaging and to minimize their effect on the surgical workflow, one solution could be the limitation of the movement range of x-ray source and image detector to ensure free access to the patient and to reduce the required imaging time. The so called limited angle tomography is exemplary shown in Figure 3.

A volumetric imaging technique which is not enclosing the object of interest is the digital tomosynthesis, mainly used for breast imaging. Only a small angle range of the rotational or translational x-ray source movement is needed, but the produced field of depth of the images is limited and objects outside of the reconstructed plane appear blurred [De07].

ISBN 978-3-88579-286-4

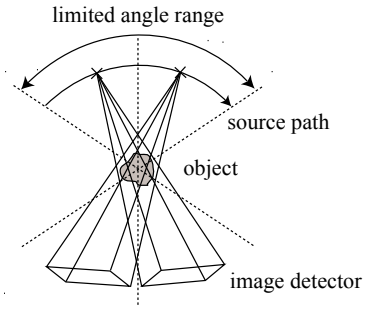

Figure 3: Example of limited angle tomography

In [Tu83] the condition for a complete x-ray source trajectory and an exact tomographic volume reconstruction is described. This completeness condition states that a volume point can be exactly reconstructed, if every plane through this point intersects the x-ray source trajectory at least once. In [Sc01] a visual method to proof the completeness of X-ray source trajectories regarding a volume is shown. Depending on the x-ray source trajectory surfaces are drawn within a sphere which represents the volume that has to be reconstructed. If the surfaces fill the sphere sufficiently the source trajectory is complete.

Using Tuy's condition an x-ray source trajectory can be classified in a complete or incomplete trajectory. Because limited angle tomographies do not fulfil Tuy's condition such x-ray source trajectories are incomplete and an exact volume reconstruction is not achievable. But if the movement range of the x-ray source trajectory is limited, it is important to know how the source trajectory has to be designed within the possible angle range to achieve the maximal achievable reconstruction quality.

The accuracy of limited angle tomographies is difficult to predict. Using an algebraic technique the volume reconstruction can be regarded as solving a linear equation system. If the angle range during the image acquisition is limited the system is underdetermined and there is no unique solution. This leads to a decreased reconstruction quality with image artifacts in the volume To evaluate the reconstruction quality of limited angle tomographies, reconstruction algorithms and computer generated phantoms are used to simulate and calculate the resulting accuracies (for example in [RPS04]). But this evaluation of an x-ray source trajectory by comparing reconstructed volumes is time-consuming, depends on the used reconstruction algorithms and is not usable for a mathematical optimization of the x-ray source trajectory. A method to predict the capability of defined limited angle and limited data tomographies without using reconstruction algorithms is shown in [CN01]. With a defined resolution function the reconstruction accuracy of single features is predicted based on the used projections. An estimation of the total achievable reconstruction quality of an image acquisition trajectory is not described.

ISBN 978-3-88579-286-4

For 3D C-arm imaging special x-ray source trajectories have been developed, e.g. a closed sinusoid trajectory to enlarge the volume region that satisfies Tuy's condition [Ya06], a horizontal trajectory to scan the human anatomy during weight bearing [Ma11] and a wobble trajectory to improve the image quality for the limited angle range [TL07]. In [BGS10] an optimization method of the C-arm acquisition trajectory has been developed for rotational coronary venography. Here a patient-independent cost function was defined to minimize the overlapping and the foreshortening of specific vessel segments of the coronary tree.

In this article we present the development of a new image acquisition trajectory for 3D x-ray imaging. The acquisition trajectory was regarded as free definable. Mechanical constraints of existing 3D x-ray systems were not considered. Only the possible movement range of the x-ray source was limited to an area above the patient to ensure the free patient access. The resulting image acquisition trajectory was simulated and evaluated with an experimental set-up. Based the presented results we propose an open system concept for an intraoperative 3D x-ray scanner.

2 Methods

Our development of an image acquisition trajectory for limited angle tomography is based on two methods:

- A method that evaluates the achievable 3D reconstruction accuracy of discrete volume points based on free definable directions of x-ray projections.
- A method for optimization of directions of x-ray projections to maximize the achievable 3D reconstruction accuracy based on the evaluation method.

2.1 Quality evaluation of directions of x-ray projections

Our evaluation method computes the achievable reconstruction quality of a volume element based on defined x-ray projections from different directions, independent of reconstruction algorithms. The method regards the grade of determinability of the volume density changes depending on a defined set of directions of x-ray projections. The density changes inside a volume can be described by gradients with a location and direction. It can be observed that the x-ray image projections of volume density changes (gradients) depend on the angle between the gradients and the x-ray beam. Based on this basic observation we derived a quality evaluation function q from the radon transform. A detailed derivation of this quality function and a comparison to the accuracy of simulated volume reconstructions is shown in [St10a]. The quality value q of a gradient $\boldsymbol{\theta}$ at a volume point $\mathbf{p}$ is defined as the sine of the angle φ between the gradient direction and the x-ray beam from source position $\mathbf{s}$ through $\mathbf{p}$.

$$q(\mathbf{p},\mathbf{s},\boldsymbol{\theta}) = \sin(\varphi) = \sin\left(\left|\arccos\left(\boldsymbol{\theta}\cdot\frac{\mathbf{p}-\mathbf{s}}{\|\mathbf{p}-\mathbf{s}\|}\right)\right|\right)$$

For a set of projections from different directions through point **p**, each gradient at this point is weighted with the maximal quality value of all given x-ray source positions.

$$q(\mathbf{p},\boldsymbol{\theta}) = \max\left(q(\mathbf{p},\mathbf{s}_i,\boldsymbol{\theta}) \mid i \in \{1,2,...,N_s\}\right)$$

This value $q(\mathbf{p}, \boldsymbol{\theta})$ describes an upper bound of the determinability of gradient $\boldsymbol{\theta}$ at point **p** by a defined x-ray source trajectory consisting of several source positions $\mathbf{s}_i$. The quality values $q(\mathbf{p}, \boldsymbol{\theta}_j)$ are calculated for all gradient directions $\boldsymbol{\theta}_j$, $j \in 1..N_g$ emanating from point **p** equally distributed in all directions. Using a unit sphere the results of $q(\mathbf{p}, \boldsymbol{\theta}_j)$ can be visualized considering the point **p** in the center of the sphere and the gradients $\boldsymbol{\theta}_j$ emanating from **p** in all directions to the sphere surface [SK97] (Figure 4). At the intersection points of the gradients $\boldsymbol{\theta}_j$ with the sphere surface the respective quality values are illustrated by shades of gray. The directions of x-ray projections are defined by x-ray source positions $\mathbf{s}_i$ on the sphere surface through the volume point **p** in the sphere center. The image detector is assumed to be aligned at the opposite side of x-ray source position **s**. The gray scale of the sphere surface shows the quality $q(\mathbf{p}, \boldsymbol{\theta}_j)$ of the gradients $\boldsymbol{\theta}_j, j \in$ 1..1000, emanating from the center equally distributed in all directions to the surface of the sphere. The dark areas represent gradient directions, which are not sufficiently determinable by the used x-ray source positions on the sphere surface.

In Figure 4a a *gradient unit sphere* is shown for one single image projection. The gradients in the same or opposite direction of the x-ray beam from source position $\mathbf{s} = (0,0,1)^T$ through point $\mathbf{p} = (0,0,0)^T$ have low quality values (dark surface areas). Gradients perpendicular to the x-ray beam are determinable with a high quality values (light-colored surface areas). In Figure 4b the gradient unit sphere is exemplary shown for $N_s = 10$ x-ray source positions on a circular 120° trajectory. The dark surface area of the sphere shows the gradient directions with a low determinability by the used x-ray source positions.

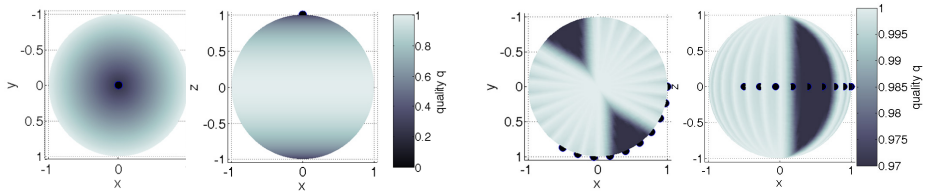

a) b)

Figure 4: a) *Gradient unit sphere* for one single projection from x-ray source position $\mathbf{s} = (0,0,1)^T$ through point $\mathbf{p} = (0,0,0)^T$ in the center of the sphere; the gray scale of the sphere surface describes the quality values $q(\mathbf{p}, \boldsymbol{\theta}_j)$ of the gradients $\boldsymbol{\theta}_j$ emanating from the center $\mathbf{p} = (0,0,0)^T$ to the surface of the sphere; b) Gradient unit sphere for 10 x-ray source positions on a 120° circular trajectory; the points represent the x-ray source positions.

2.2 Optimization of directions of x-ray projections

To ensure free patient access during image acquisition, a complete x-ray source trajectory with a fully 360° or 180° circular rotation of x-ray source and image detector around the patient is not applicable. Therefore we limited the possible x-ray source movement range and optimized the directions of x-ray projections using our quality evaluation method [St10b]. To minimize the calculation complexity only one point **p** in the volume center is considered, but the method can also be applied to a discrete volume grid consisting of several separate volume points. The reconstruction quality at volume point **p** is determined by the arithmetic mean value $q(\mathbf{p})$ of all gradient directions.

$$q(\mathbf{p}) = \frac{1}{\pi}\int_0^{\pi}\frac{1}{2\pi}\int_0^{2\pi} q(\mathbf{p},\boldsymbol{\theta}(\phi,\vartheta))\,d\phi\,d\vartheta \quad \text{with} \quad \boldsymbol{\theta}(\phi,\vartheta) = (\sin\vartheta\cos\phi, \sin\vartheta\sin\phi, \cos\vartheta)^T$$

Based on this quality $q(\mathbf{p})$ we defined the error function ε to optimize the directions of x-ray projections within predefined limited angle ranges.

$$\varepsilon = (1 - q(\mathbf{p}))^2$$

In Figure 5 we optimized exemplary 10 directions of x-ray projections using the MATLAB Optimization Toolbox and regarding N_g = 1000 gradients. The limited angle ranges are defined by spherical caps in relation to the volume point in the sphere center. We used angle ranges of 40°, 80°, 120° and 360° shown as green spherical caps in the upper row of Figure 5. The optimized x-ray source positions $\mathbf{s}_i$ are denoted by black dots on the sphere surface in the middle row and in sphere coordinate in the lower row of Figure 5. The optimized directions of x-ray projections are defined by the source positions $\mathbf{s}_i$ on the sphere surface and the regarded volume point **p** in the center of the sphere. The limited angle range is marked by a black line. Depending on the optimized source positions $\mathbf{s}_i$ the sphere surface shows the gray scaled quality values (as shown in Figure 4).

Using an unlimited angle range of 360° (Figure 5 right column) the source positions were aligned equally distributed along a circular line of 180°, similar to a conventional C-arm x-ray source trajectory. The optimization within limited angle ranges of 40°, 80° and 120° leads to an x-ray source positioning at the area boundary of the spherical caps. With a growing angle range the insufficiently determinable gradient directions are decreasing. Because of the fixed number of 10 projections the distances of the source positions along the area boundary increase with a growing angle range. This increased undersampling leads to dark streaks in the area of determinable gradient directions by the optimized source positions.

Because of the undersampling one x-ray source position was optimized in the center of the spherical cap using an angle range of 120° and 10 source positions. This central source position leads to a bright horizontal streak at ϑ = 90° because of the good determinabilty of perpendicular gradient directions (see the middle and lower row of an angle range of 120° in Figure 5).

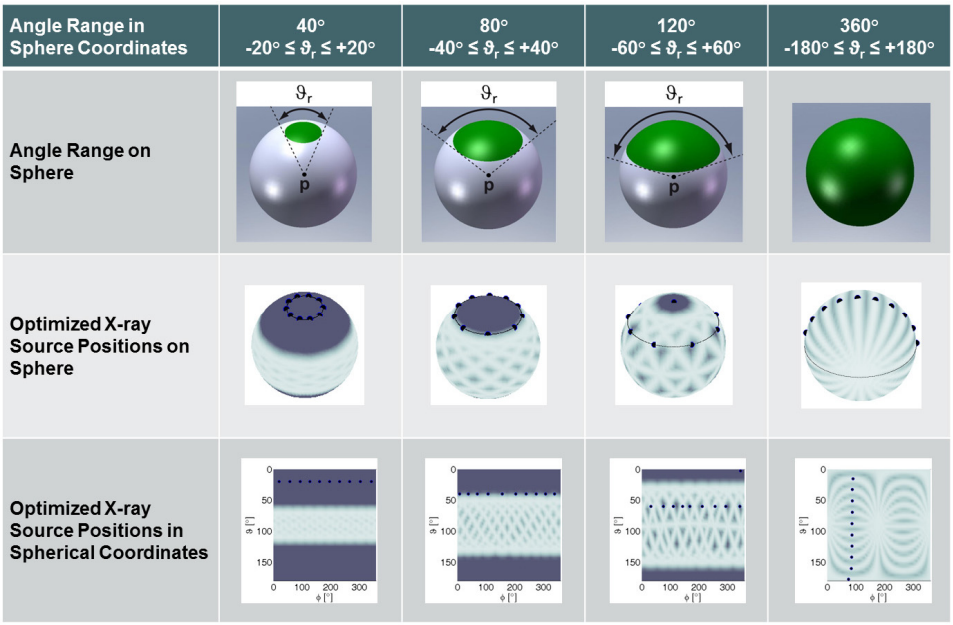

Figure 5: Optimization of 10 x-ray source positions within different angle ranges regarding the achievable reconstruction quality $q(\mathbf{p})$ at volume point $\mathbf{p}$ in the center of the sphere. The upper row shows the used angle ranges marked as green spherical caps. The middle and lower row show the optimized x-ray source positions $\mathbf{s}_i$ denoted by black dots on the sphere surface and in spherical coordinates.

2.3 Orbital x-ray source trajectory

The limitation of the angle range of directions of x-ray projections leads to insufficient determinable gradient directions (visualized by the dark surface areas on the sphere in Figure 5). This is independent of the number and the arrangement of source positions, because required directions of x-ray projections for a complete x-ray source trajectory are outside of the limited angle range. Therefore an exact 3D reconstruction is not achievable in limited angle tomography.

To achieve the maximal reconstruction accuracy for a predefined limited angle range our evaluation function and optimization method are useful to design an x-ray source trajectory within the possible angle range. Using a limited number of source positions their arrangement within the possible angle range is essential regarding the determinabilty of the volume density changes (gradients).

If the angle range is limited in form of spherical caps above the regarded volume point, the maximal possible reconstruction quality is achieved by aligning a sufficient number of source positions at the area boundary of the spherical caps (Figure 6a). In spite of still existing insufficient determinable gradient directions caused by the limited angle range, such an orbital x-ray source trajectory allows an optimal reconstruction quality for these defined angle range limitations. Figure 6b shows the orbital x-ray source trajectory derived from our optimization results, where the x-ray source is circular rotating in one plane above the volume.

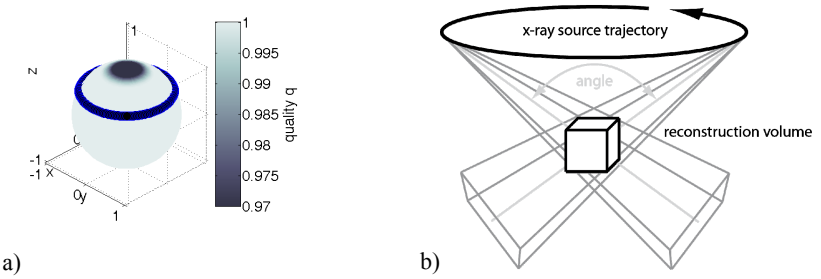

a) b)

Figure 6: Visualization of the orbital x-ray source trajectory derived from the optimization results: a) On the *gradient unit sphere* at the area boundary of the spherical cap with an angle range of 120°; b) Scanning a cubic volume

3 Results

We analyzed and evaluated our orbital x-ray source trajectory by simulations with our 3D reconstruction software. According to defined image acquisition trajectories the simulation software calculates artificial projection images of mathematical defined phantoms, e.g. the Shepp-Logan head phantom [YYW04]. Based on the calculated projection images the scanned phantom was reconstructed using the simultaneous algebraic reconstruction technique (SART).

The first row in Figure 7 shows the *gradient unit sphere* of our orbital x-ray source trajectory with an exemplary opening angle of 120° in three orthogonal views. The second row shows the reconstruction result of the Shepp-Logan head phantom using 180 x-ray projection images and the third row the original mathematical defined phantom. For projection image calculation the phantom was located in the center of the sphere and the image detector was aligned perpendicularly to the central x-ray beam from the source positions through the volume. The size of both volumes is 256^3 voxel with a voxel size of 0.01 mm. The sagittal view shows the volume slice y = 128, the axial view volume slice x = 141 and the coronal view volume slice z = 104.

Comparing the reconstructed volume with the original head phantom, geometrical distortions at the top and bottom are visible in the sagittal and axial view. These artifacts are caused by the limited angle range and occur at density changes in vertical directions of the volume. Figure 7 shows the correlation between the dark areas of the *gradient unit sphere* and these artifacts in the reconstructed volume. The absence of projection images in horizontal direction lead to insufficiently determinable density changes in vertical direction. Using the Shepp-Logan head phantom such vertical gradients are located at the top and bottom of the elliptical-shaped head.

To minimize these artifacts and to improve the image quality specialized algorithms for limited angle tomography have been developed. A significant improvement of the reconstruction quality is for example shown in [SKP06] and [VLC07] by minimizing the total variation of the reconstruction. Based on the previous knowledge about the insufficiently determinable volume gradients and the existing approaches to handle limited angle tomographies, our goal in future work is to develop an iterative reconstruction algorithm which is adapted and optimized to the orbital x-ray source trajectory.

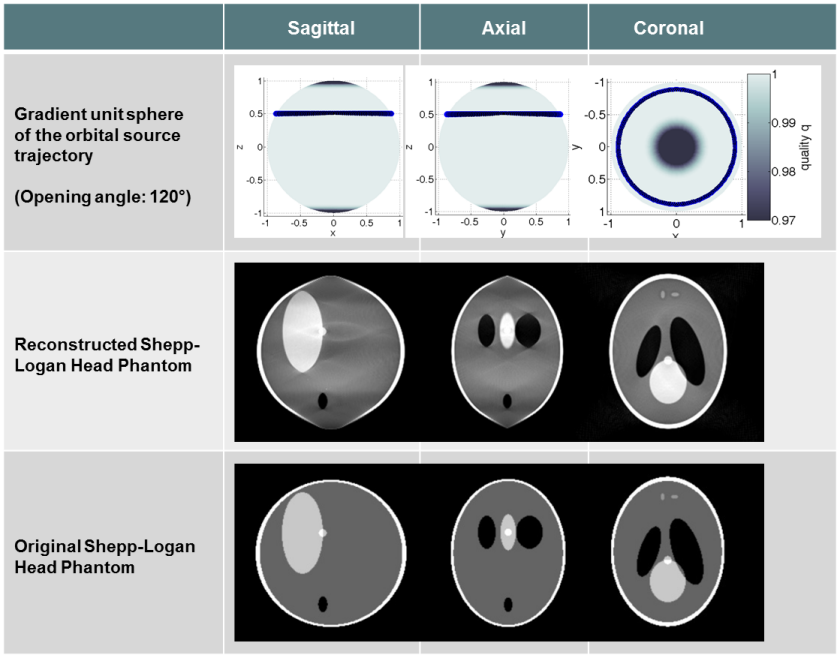

Figure 7: Simulated orbital x-ray source trajectory: X-ray source positions on a gradient unit sphere with an opening angle of 120° (upper row); Volume slices of the reconstructed Shepp-Logan head phantom (middle row from left to right: y = 128, x = 141, z = 104); Volume slices of the original Shepp-Logan head phantom (lower row from left to right: y = 128, x = 141, z = 104)

To verify the simulation results we built up an experimental set-up consisting of an x-ray source, a digital flat-panel detector and a robotic arm (Figure 8). To realize a defined image acquisition trajectory the test object was mounted on the robotic arm and moved between the fixed x-ray source and the fixed image detector to acquire projection images of the test object from different directions.

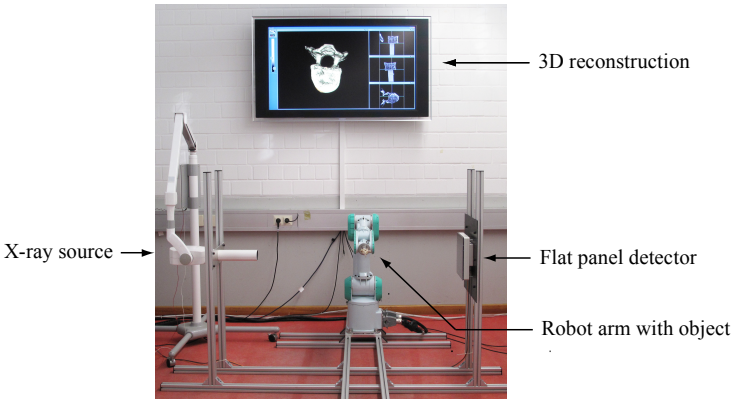

Figure 8: Experimental set-up to realize and evaluate the orbital x-ray source trajectory

We analyzed the spatial resolution of the orbital x-ray source trajectory with a drill hole test phantom (according to [Ka95]) with drill hole diameters from 0.4 mm to 2.0 mm (Figure 9). Drill holes with the same diameter are radial aligned with distances between the holes equal to the hole diameter. This allows the determination of the spatial resolution in line pairs per centimeter (lp/cm). We achieved a resolution of 12.5 line pair per cm (lp/cm) in the axial slice of the reconstructed volume using an opening angle of 120° between the volume center and the orbital x-ray source trajectory above the volume.

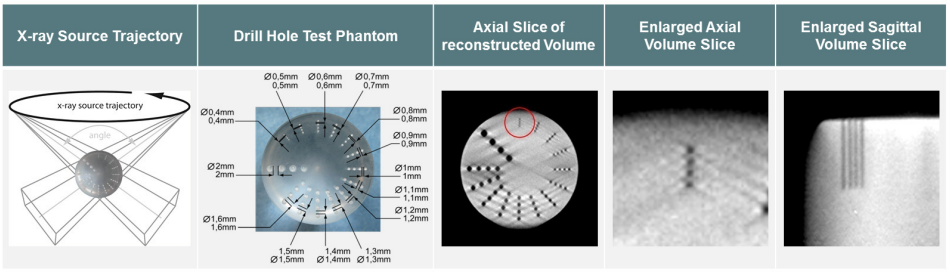

Figure 9: Spatial resolution analysis in the reconstructed axial slice using a drill hole test phantom; 12.5 lp/cm (0.4 mm holes) are clearly visible using an opening angle of 120° between the volume center and the orbital x-ray source trajectory above the volume

The clinical usability of the orbital image acquisition method was analyzed exemplarily for a spine surgery application. Therefore we used human vertebral bodies of thoracic and lumbar spine. Figure 10 shows the reconstruction of a thoracic vertebral body. The reconstructed volume has a high image quality and the pedicles and the spinal canal of the vertebral body are clearly visible.

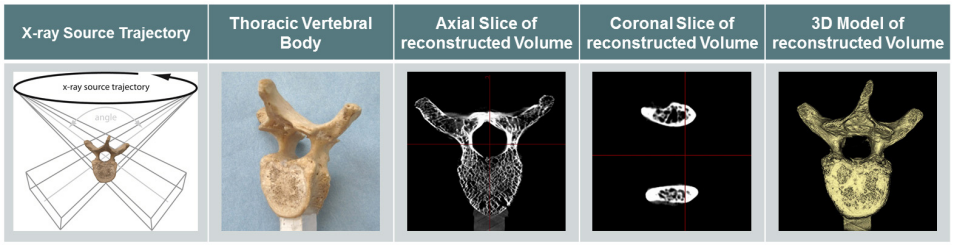

Figure 10: 3D scan of a thoracic vertebral body using the orbital x-ray source trajectory and an opening angle of 120°.

Using a synthetic vertebral body with two inserted metallic screws, we analyzed the resulting image quality of our orbital x-ray source trajectory in comparison to a conventional C-arm trajectory. In both studies we used 181 projection images of the prepared vertebral body equally distributed over the whole trajectory paths and exactly the same reconstruction parameters.

Figure 11 shows the 3D reconstruction results of our orbital and the conventional C-arm x-ray source trajectory. Because pedicle screws are often located in the C-arm rotation plane of x-ray source and image detector, there are significant artifacts between the screws in the reconstructed volume. This can lead to unusable 3D images if the verification of the correct implant position in relation to the spinal canal inside of the vertebral body is not possible (first row in Figure 11).

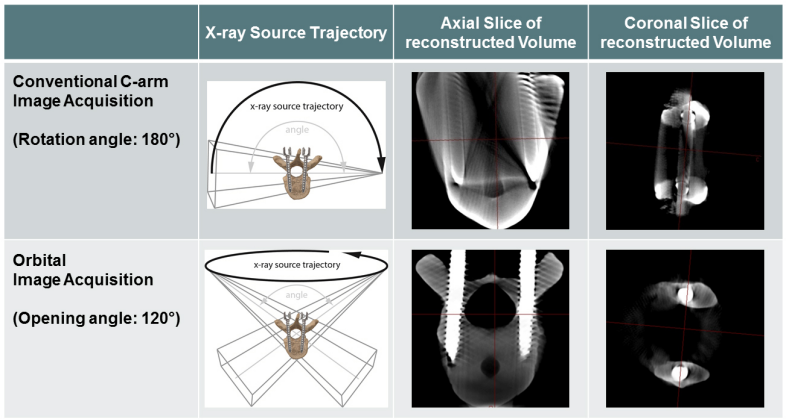

Figure 11: Comparison of our orbital x-ray source trajectory with a conventional C-arm image acquisition method using a synthetic vertebral body with two inserted pedicle screws

The second row of Figure 11 shows the reconstruction result using our orbital x-ray source trajectory above the scanned volume with an opening angle of 120°. Because x-ray source and image detector are not rotating in one single plane during image acquisition, the metal artifacts are reduced significantly in comparison to conventional 180° circular c-arm rotations. The spinal canal of the vertebral body is clearly visible und the exact position of the two screws can be verified.

Based on the simulation and experimental results we propose a new system concept of an intraoperative 3D x-ray scanner to realize our orbital image acquisition method. To improve the intraoperative usability of 3D x-ray imaging and to ensure free access to the patient we break the rigid configuration of x-ray source and image detector. The 3D x-ray scanner ORBIT consists of an x-ray source mounted on a robotic arm, a digital flat-panel detector fixed on or integrated in the patient table and a control and monitor cart (Figure 12). Because in this concept the image detector is fixed and not perpendicular to the central x-ray beams, we simulated the orbital image acquisition method also with a static image detector parallel to the plane of the orbital x-ray source movement. Using our simulation environment with the SART algorithm the image quality was identical to the previously presented results.

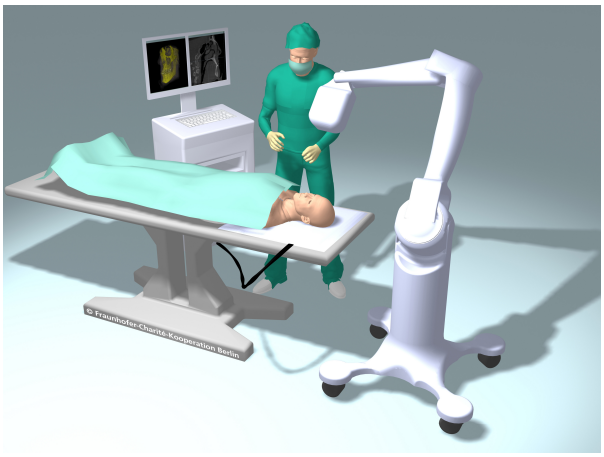

Figure 12: ORBIT – Open x-ray scanner for image guided interventional surgery consisting of an x-ray source on a robotic arm, a fixed digital flat-panel detector on the patient table and a control and monitor cart

In future work we realize a first prototype of ORBIT at the Charité – Universitätsmedizin Berlin in cooperation with Ziehm Imaging GmbH to perform experimental evaluations and further developments regarding image quality and clinical usability.

4 Conclusion

To improve the usability of intraoperative 3D x-ray imaging by ensuring free access to the patient, we propose a new system concept with an orbital image acquisition method. The development of the orbital x-ray source trajectory is based on the optimization of directions of x-ray projections within a limited angle range regarding the achievable reconstruction quality. A limited angle range of the x-ray source trajectory allows free access to the patient but leads to artifacts in the 3D reconstruction. Using our evaluation method and the *gradient unit sphere* of an x-ray source trajectory within a limited angle range, the characteristic of these artifacts is predictable and their effects can be minimized. In future work our goal is to optimize the 3D reconstruction quality for the limited orbital x-ray source trajectory and to analyze the resulting radiation exposure in comparison to the conventional circular imaging technique. To perform further developments we build up a first prototype of the open 3D x-ray scanner ORBIT at the Charité - Universitätsmedizin Berlin.

Acknowledgements

This work is supported by the German Federal Ministry of Education and Research (BMBF), grant #01EZ1115.

References

[Be97] Berlemann, U.; Heini, P.; Müller, U.; Stoupis, C.; Schwarzenbach, O.: Reliability of pedicle screw assessment utilizing plain radiographs versus CT reconstruction. In: European spine journal (1997), Vol. 6, S. 406-411.

[Be09] Beck, M.; Moritz, K.; Gierer, P.; Gradl, G.; Harms, C.; Mittlmeier, T.: Intraoperative Control of Pedicle Screw Position using Three-Dimensional Fluoroscopy. A Prospective Study in Thoracolumbar Fractures. In: Zeitschrift für Orthopädie und Unfallchirurgie 2009, Vol. 147, Nr. 1, S. 37–42.

[BGS10] Bi, J.; Grass, M.; Schäfer, D.: Optimization of acquisition trajectories for 3D rotational coronary venography. Int J Comput Assist Radiol Surg. 2010, vol. 5, S. 19–28, DOI 10.1007/s11548-009-0398-7.

[CN01] Clackdoyle, R.; Noo, F.: Cone-Beam Tomography from 12 Pinhole Vertices. IEEE Nuclear Science Symposium Conference Record, vol. 4, S. 1874 - 1876, 2001.

[De07] Deller, T.; Jabri, K. N.; Sabol, J. M.; Ni, X.; Avinash, G.; Saunders, R.; Uppaluri, R.: Effect of Acquisition Parameters on Image Quality in Digital Tomosynthesis. In: Physics of Medical imaging, Proc. of SPIE, Vol. 6510, 65101L-1, 2007.

[Ka95] Kalender, W.A.: Thin-Section Three-dimensional Spiral CT: Is Isotropic Imaging Possible? In: Radiology 1995, vol. 197, Nr. 3, S. 578-580.

[Ke09] Kendoff, D.; Citak, M.; Gardner, M. J.; Stübig, T.; Krettek, C.; Hüfner, T.: Intraoperative 3D Imaging: Value and Consequences in 248 cases. In: Journal of Trauma Injury Infection and Critical Care 66(1); S. 232-238, 2009.

[LSG10] Lotfinia, I.; Sayahmelli, S.; Gavami, M.: Postoperative Computed Tomography Assessment of Pedicle Screw Placement Accuracy. In: Turkish Neurosurgery 2010, Vol. 20, No 4, S. 500-507.

[Ma11] Maier, A.; Choi, J.-H.; Keil, A.; Niebler, C.; Sarmiento, M.; Fieselmann, A.; Gold, G.; Delp, S.; Fahrig, R.: Analysis of Vertical and Horizontal Circular C-Arm Trajectories. Physics of Medical Imaging 2011, Proc. Of SPIE Vol. 7961, 796123, doi 10.1117/12.878502.

[RPS04] Ramamurthi, K.; Prince, J. L.; Strobel, N.: Exact 3d conebeam reconstruction from projections obtained over a wobble trajectory on a c-arm. IEEE International Symposium on Biomedical Imaging (ISBI), vol. 1, S. 932 - 935, 2004.

[Sc01] Schomberg, H.: Complete Source Trajectories for C-Arm Systems and a Method for Coping with Truncated Cone-Beam Projections. Proc. 6th International Meeting on Fully Three-Dimensional Image Reconstruction in Radiology and Nuclear Medicine, 2001.

[Sc04] Schnake, K. J.; König, B.; Berth, U.; Schroeder, R. J.; Kandziora, F.; Stöckle, U.; Raschke, M.; Haas, N. P.: Accuracy of CT-based navigated thoracic pedicle screws in comparison to a conventional technique. In: Unfallchirurg; Springer Verlag 2004, Nr. 107, S. 104–112.

[SK97] Saff, E. B.; Kuijlaars, A. B. J.: Distributing Many Points on a Sphere. In: The Mathematical Intelligencer, Vol. 19, No. 1, S. 5-11, 1997.

[SKP06] Sidky, E. Y.; Kao, C.-M.; Pan, X.: Accurate image reconstruction from few-views and limited-angle data in divergent-beam CT. In: Journal of X-Ray Science and Technology (2006), vol. 14, Nr. 2, S. 119-139.

[St10a] Stopp, F.; Winne, C.; Jank, E.; Keeve, E.: Quality Evaluation of Image Recording Strategies for Limited Angle Tomography. In: Tsinghua Science and Technology, ISSN 1007-0214, Vol. 15, No. 1, pp. 25-29, 2010.

[St10b] Stopp, F.; Winne, C.; Käseberg, M.; Keeve, E.: Optimization of directions of x-ray projections for limited angle tomography. In: Biomedizinische Technik 55 (2010), Supplement 1, ISSN 0013-5585.

[TL07] Tita, R.; Lüth, T. C.: Free isocentric 3d imaging and a novel approach for wobble trajectories using a modified standard c-arm. IEEE EMBS, S. 4418 - 4421, 2007.

[Tu83] Tuy, H. K.: An inversion formula for cone-beam reconstruction. SIAMJ. Appl. Math., vol. 43, S. 546–552, 1983.

[VLC07] Velikina, J.; Leng, S.; Chen, G.-H.: Limited view angle tomographic image reconstruction via total variation minimization. Proc. SPIE, vol. 6510, 2007.

[Ya06] Yang, H.; Li, M.; Koizumi, K.; Kudo, H.: Closed Sinusoid Trajectory for C-Arm CT Imaging. IEEE Nuclear Science Symposium Conference Record, M14-456, S. 3480-3484, 2006.

[YYW04] Yu, H., Ye, Y., Wang, G.: Katsevich-type algorithms for variable radius spiral cone-beam CT. Proceedings of SPIE, Vol. 5535, S. 550 - 557, 2004.

ISBN 978-3-88579-286-4